This is an open access article published under a Creative Commons Attribution (CC-BY) License, which permits unrestricted use, distribution and reproduction in any medium, provided the author and source are cited.

CRYSTAL GROWTH & DESIGN

Article

pubs.acs.org/crystal

Photocatalytic Oxygen Evolution from Cobalt-Modified Nanocrystalline $BiFeO_3$ Films Grown via Low-Pressure Chemical Vapor Deposition from β-Diketonate Precursors

Savio J. A. Moniz,[*,†,‡] David Pugh,[§,⊥] Christopher S. Blackman,[*,‡] Junwang Tang,[†] and Claire J. Carmalt[‡]

[†]Department of Chemical Engineering, University College London, Torrington Place, London WC1E 7JE, United Kingdom

[‡]Department of Chemistry, University College London, 20 Gordon Street, London WC1H 0AJ, United Kingdom

[§]Department of Chemistry, University of Southampton, Highfield, Southampton SO17 1BJ, United Kingdom

S *Supporting Information*

ABSTRACT: $BiFeO_3$ is an interesting multifunctional narrow band gap semiconductor that exhibits simultaneous multiferroic, photovoltaic, and photocatalytic behavior. Hence there is much interest in the growth of thin films of $BiFeO_3$ via chemical vapor deposition (CVD); however, the number of suitable bismuth precursors is severely limited. A series of homoleptic bismuth(III) β-diketonate complexes were synthesized via simple room temperature ligand-exchange reactions from $[Bi(N(SiMe_3)_2)_3]$ and free diketonate ligands, which yielded the crystal structure of $[Bi(acac)_3]$ as a 1-D polymer. We attempted to use these complexes for low pressure CVD (LPCVD) growth of $BiFeO_3$ films with $[Fe(acac)_3]$; however, all bismuth complexes exhibited poor volatilities and decomposition characteristics, and as a result film growth was unsuccessful. Subsequently, the volatile alkoxide $[Bi(O^tBu)_3]$, with $[Fe(acac)_3]$, was used to grow dense $BiFeO_3$ films via low pressure CVD. The $BiFeO_3$ films possessed multiferroic properties at room temperature and exhibited activity for visible light-driven water oxidation in the presence of a Ag^+ electron scavenger, which improved significantly when modified with a cobalt surface cocatalyst. The increase in activity, probed by time-resolved photoluminescence spectroscopy, was attributed to improved charge carrier separation arising from the in-built internal electric field of $BiFeO_3$ in addition to the presence of an efficient cobalt oxygen evolution catalyst.

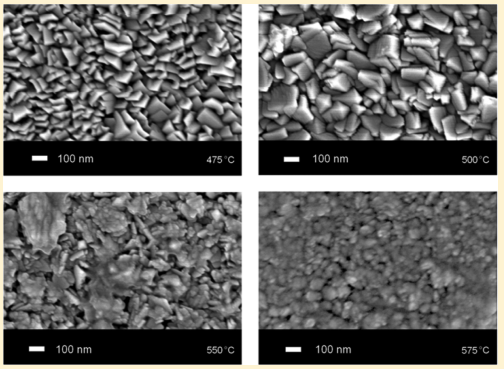

INTRODUCTION

Bismuth(III) oxide is a common component of ferroelectric, multiferroic, and superconducting metal oxide films. Perovskite bismuth ferrite ($BiFeO_3$, "BFO") is a promising multifunctional material that possesses a direct band gap of approximately 2.2 eV, providing interesting photovoltaic and photocatalytic properties, and also exhibits simultaneous ferroelectric and ferromagnetic ordering (multiferroic). In addition it has been demonstrated that, due to the ferroelectric polarization in BFO, the electron−hole separation is promoted.[1−3] Solar-driven catalysis on semiconductors to produce clean chemical fuels, such as hydrogen, is widely considered as a promising route to mitigate environmental issues caused by the combustion of fossil fuels and to meet increasing worldwide demands for energy. However, the oxygen evolution reaction (OER) is challenging because production of one molecule of gaseous oxygen requires four holes (oxidize two molecules of water), and occurs on a time scale approximately 5 orders of magnitude slower than H_2 evolution, proven in both natural and artificial photosynthesis.[4] Furthermore, there are few visible light-driven semiconductors that satisfy the thermodynamic and kinetic barriers for water splitting. We have recently shown that $BiFeO_3$ exhibits the required overpotential for water oxidation due to its positive valence band (VB) position of 2.3 V vs RHE and produces gaseous oxygen (under an applied bias) in a photoelectrochemical cell.[5]

A potential method for large scale growth of bismuth-containing films is via chemical vapor deposition (CVD). In general, commercially available precursors are preferred for use in CVD, and for deposition of $BiFeO_3$, the iron precursor $[Fe(acac)_3]$ (acac = acetylacetonate) has appreciable stability, appreciable volatility, and relatively low-cost. Deposition of complex oxides such as $BiFeO_3$ via CVD requires use of dual metal precursors, and due to the difficulty of controlling incorporation of both metals the use of ligand-matched precursors is advisible due to the generally similar chemical behavior displayed. In addition, the use of ligand-matched precursors is preferred to reduce the likelihood of unwanted gas-phase reactions and ligand rearrangement (scrambling) occurring between complexes during thermal CVD.[6] The vast majority of CVD precursors to metal oxide films containing heavy elements such as bismuth are based on metal β-

Received: March 7, 2016
Revised: May 6, 2016
Published: May 24, 2016

 © 2016 American Chemical Society

DOI: 10.1021/acs.cgd.6b00370
Cryst. Growth Des. 2016, 16, 3818−3825

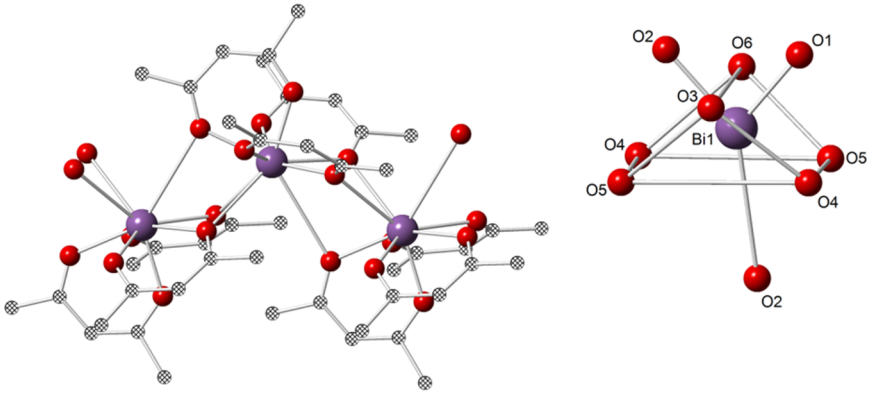

Figure 1. (a) Representation of the polymeric nature of $[Bi(acac)_3]$; (b) representation of the 9-coordinate distorted tricapped trigonal prism coordination sphere at Bi, showing the vertices of the distorted trigonal prism and the capping atoms. Atom colors: Bi = purple, O = red, C = gray.

diketonates, as they stabilize the metal center toward oligomerization, and in addition are typically easy to handle, are low cost, and are usually stable when vaporized.[7] However, there are relatively few volatile bismuth precursors available for conventional thermal CVD processes at atmospheric pressure (AP)- and low pressure (LP)-CVD, and the commercially available β-diketonate $[Bi(thd)_3]$ (thd = 2,2,6,6-tetramethyl-3,5-heptanedionate) suffers from poor decomposition characteristics.[8] Previously, we synthesized $[Bi(dbm_3)]_2$ (dbm = dibenzoylmethane) using a novel ligand-exchange reaction with $[Bi(N(SiMe_3)_2)_3]$ and the free ligand under extremely mild conditions;[9] however, while it is an excellent precursor for aerosol-assisted CVD, it is not sufficiently volatile for use in AP- or LPCVD.

Herein, we report the synthesis of three novel homoleptic bismuth(III) β-diketonate complexes, together with the crystal structure of $[Bi(acac)_3]$, and we assess their suitability for CVD film growth. We demonstrate the first use of $[Fe(acac)_3]$ for LPCVD growth of $BiFeO_3$ films, but only in conjunction with $[Bi(O^tBu)_3]$ due to the subsequent poor volatilities and decomposition characteristics of the bismuth diketonates. Films were fully characterized and were able to photo-oxidize water to evolve gaseous oxygen in the presence of a sacrificial electron acceptor ($AgNO_3$) and a cobalt cocatalyst.

EXPERIMENTAL SECTION

Precursor Synthesis. Details of the syntheses and single crystal X-ray diffraction studies of the bismuth β-diketonate complexes can be found in the Supporting Information.

Film Growth. Nitrogen (99.96%, 50 sccm) was obtained from BOC and used as a carrier gas as supplied. A base pressure of 2×10^{-3} mbar was achieved before use, to ensure, as far as possible, that no air and moisture remained in the system. The total reactor pressure was varied via the use of a mechanical throttle valve. Each deposition was carried out for 1 h. Films were deposited on borosilicate glass microscope slides (3 cm × 2 cm) or platinized silicon wafers. Nitrogen (99.96%) was obtained from BOC and used as supplied. $[Fe(acac)_3]$ (99.9%) was obtained from Sigma-Aldrich Ltd. and used as supplied. Bismuth *tert*-butoxide, $[Bi(O^tBu)_3]$, was synthesized according to the literature via the metathesis reaction between $BiCl_3$ and three molar equivalents of NaO^tBu.[10] A slight excess of bismuth precursor was used in order to compensate for bismuth evaporation at high temperatures due to the low melting point of bismuth (271 °C). $[Bi(O^tBu)_3]$ (150 mg, 0.35 mmol) and $[Fe(acac)_3]$ (100 mg, 0.28 mmol) were used for each deposition, and the bubbler temperatures were set at 110 and 160 °C, respectively.

Film Analysis. X-ray diffraction was carried out using a Bruker-AXS D4 powder diffractometer in reflection geometry using Cu Kα radiation (λ = 1.54056 Å) on a rotating sample holder in the range 10−70° 2θ, 0.05° step size, with 2 s per step. Phase information was obtained from the Diffrac*plus* EVA program suite (Version 2) and ICSD. Scanning electron microscopy (SEM) was used in order to examine surface morphology and films thickness. Images were obtained on a Jeol JSM-6301F field emission microscope at 5 kV, after coating samples with an ultrathin layer of gold to prevent charging. Quantitative analyses of bismuth and iron were carried out via WDX using a Philips XL30ESEM machine operating at 10 kV, equipped with an Oxford Instruments INCA detector. Films were carbon coated prior to analysis to prevent charging. XPS analysis was performed using a Kratos AXIS Ultra machine with a delay line detector under a pressure of 10^{-9} Torr. A monochromated Al−K_α X-ray source producing a full width at half-maximum (fwhm) on the Ag $3d_{5/2}$ peak of 0.48 eV was used. Raman spectra were acquired using a Renishaw Raman 1000 System using a helium−neon laser wavelength of 514.5 nm at room temperature (20 °C) and liquid nitrogen temperature (−195 °C) using a cold stage and temperature controller equipped with a cryo pump. AFM analysis was performed using a Veeco Dimension 3100 machine in intermittent contact mode. UV−vis spectra were recorded in transmission mode over the range 300−2500 nm using a PerkinElmer Lambda 950 photospectrometer. Magnetism measurements (M-H hysteresis and ZFC-FC magnetization) were conducted using a Quantum Design SQUID Vibrating Sample Magnetometer (VSM) with a maximum field setting of 7 T (70000 Oe). Films were mounted on a 4 mm diameter quartz rod using a vinylphenolic adhesive (code GE7031, stable up to 400 K) and suspended parallel to the magnetic field (in-plane). Time-resolved photoluminescence spectroscopy was carried out at room temperature using a LifeSpec II TCSPC fluorescence spectrometer using a laser excitation wavelength of 432 nm and 50 μs pulse duration.

Photocatalytic Oxygen Evolution. $BiFeO_3$ was tested for photocatalytic water oxidation in the presence of a sacrificial electron acceptor in the form of $AgNO_3$. The film was placed within a Teflon holder and inserted upon the base of a custom-made Pyrex reactor. 0.2 g of $AgNO_3$ was dissolved in 50 mL DI water with stirring and added to the reactor to immerse the film, area 1 cm^2. The reactor was sealed and purged with argon gas for 20 min to remove all oxygen. A 300 W Xe lamp (Newport, USA) was used to irradiate the sample; the cell was stirred vigorously to ensure oxygen bubbles were transferred to the headspace. Gas measurements were taken every hour from the headspace of the reactor and injected into a GC (Varian 430-GC, 5A mol. sieve column). A 420 nm long-pass filter (Newport, USA) was used for visible light testing. Quantum yield was calculated using a 420 nm band-pass filter and Newport power meter in line with standard protocols.[11,12]

RESULTS AND DISCUSSION

There are a number of routes to bismuth(III) β-diketonates reported in the literature; for example, the synthesis of volatile

DOI: 10.1021/acs.cgd.6b00370
Cryst. Growth Des. 2016, 16, 3818−3825

$[Bi(thd)_3]$, which has been widely used as a CVD precursor to Bi_2O_3 films, was first reported via the metathesis reaction of $BiCl_3$ and Na(thd).[13] It has also been isolated via the reflux of $BiPh_3$ and Hthd,[14] and this method has been successfully applied in the synthesis of the fluorinated bismuth β-diketonates $[Bi(hfac)_3]$[15] (hfac = hexafluoroacetylacetonate), $[BiPh(hfac)_2]$[16] and $[Bi(fod)_3]$ (fod =6,6,7,7,8,8,8-heptafluoro-2,2-dimethyl-3,5-octanedionate).[17] Recently, we reported the synthesis of dimeric $[Bi(dbm)_3]_2$ via the ligand-exchange reaction between dbmH and $[Bi(N(SiMe_3)_2)_3]$,[9] which occurred immediately; $[Bi(acac)_3]$ is insoluble in hexane, so it can be simply filtered to isolate $[Bi(acac)_3]$. Crystals suitable for single crystal diffraction were grown from a concentrated toluene solution.

$[Bi(acac)_3]$ is unusual with respect to other crystallographically characterized $[Bi(\beta\text{-diketonate})_3]$ complexes in that it exists as a 1-D coordination polymer (Figure 1). The compounds $[Bi(thd)_3]$, $[Bi(hfac)_3]$, and $[Bi(dbzm)_3]$ are all discrete dimers with 7- or 8-coordinate Bi centers and gaps in the coordination sphere of Bi, presumably where stereochemically active lone pairs are located. This effect is almost certainly steric in origin; the relatively small acac ligands can pack much closer together than other β-diketonate ligands where large substituents, such as ^{t}Bu(thd),[14,18] CF_3(hfac),[15] and Ph-(dbzm),[9] prevent the formation of extended structures. Further description of the crystal structure of $[Bi(acac)_3]$ is provided in the Supporting Information and in Figure S1.

We attempted to prepare other bismuth(III)β-diketonates using ligand-exchange reactions with $[Bi(N(SiMe_3)_2)_3]$. Synthesis of $[Bi(tfac)_3]$ (tfac =1,1,1-trifluoroacetylacetonate) was successful, resulting in *ca.* 85% yield of $[Bi(tfac)_3]$ as a white powder. Despite numerous attempts, X-ray quality single crystals of $[Bi(tfac)_3]$ could not be grown. Similarly, this ligand-exchange route worked well for preparation of $[Bi(bzac)_3]$ which was isolated in 76% yield, however X-ray quality single crystals could not be grown. All three synthesized bismuth β-diketonates were assessed for their volatility and decomposition characteristics, which are crucial for thin film growth in thermal CVD. Sublimation under reduced pressure is a simple method to screen volatility of metal−organic complexes before they can be considered for use as conventional CVD precursors. Unfortunately all three complexes were found not to be volatile over a wide range of temperatures and pressures. In particular the surprising polymeric structure of $[Bi(acac)_3]_n$ in the solid state is perhaps the most important reason why this complex possesses such low volatility. The decomposition profiles of the three bismuth complexes were assessed via DSC-TGA (Figure 2). From XRD analysis of the residues remaining in the pans from all three complexes (Figures S2 - S4), metallic bismuth was found and hence is further evidence of their poor suitability for LPCVD. Further analysis of the TGA study can be found in the Supporting Information.

Chemical Vapor Deposition Studies. Initially, we attempted the volatilization of all three bismuth β-diketonates in conjunction with the volatile iron(III) β-diketonate $[Fe(acac)_3]$ to deposit $BiFeO_3$ films via dual-source LPCVD. However, following several attempts over a range of temperatures and pressures, no films were produced, and this was attributed to bismuth precursor decomposition with no vapor transport. Consequently, we conclude that β-diketonate complexes of bismuth are generally unsuitable for use in CVD where vapor transport of the precursor is required. We

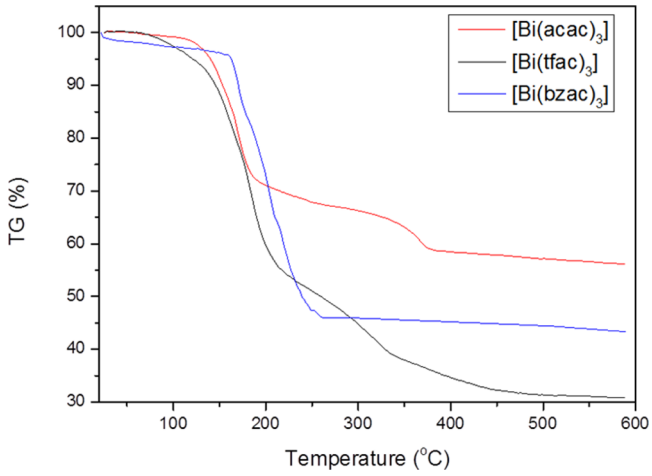

Figure 2. Decomposition profiles of $[Bi(acac)_3]$, $[Bi(tfac)_3]$, and $[Bi(bzac)_3]$ measured using TGA.

believe this finding is of significant importance to those studying the growth of bismuth-containing oxide species via CVD in terms of precursor selection. The number of volatile β-diketonate precursors for bismuth oxide films is extremely limited (only $[Bi(thd)_3]$ shows moderate volatility), and therefore, only the alkoxides $[Bi(mmp)_3]$ and $[Bi(O^tBu)_3]$ demonstrate suitable volatility and thermal stability to be used for film growth. We also attempted the growth of $BiFeO_3$ films using these diketonate complexes in conjunction with $[Fe(acac)_3]$ via a solution-based AACVD procedure, using a variety of solvents. Unfortunately, only iron oxide (α-Fe_2O_3) films were produced with no bismuth incorporation, most likely due to the poor decomposition and thermal stability of the bismuth β-diketonates. While this may be surprising given that the decomposition of $[Bi(tfac)_3]$ and $[Bi(bzac)_3]$ resulted in bismuth oxide formation from TGA studies, in fact under AACVD conditions the interaction of solvent and gas flow can adversely affect decomposition. Nevertheless, it might be possible that these complexes can yield bismuth oxides using other solution-based procedures, such as sol−gel or spin coating; however, this is beyond the scope of this study.

While we were somewhat concerned about the possibility of gas-phase ligand scrambling affecting film growth, we investigated whether an iron β-diketonate could be used with a proven volatile bismuth alkoxide for BFO growth. Subsequently we studied $[Bi(O^tBu)_3]$ in conjunction with $[Fe(acac)_3]$ to deposit $BiFeO_3$ films. The TGA traces of these precursors and their vapor pressures are plotted together in Supporting Information Figures S5 and S6. Without the use of oxidizing gas (Lines 1−4, Table 1) as coreactant, dark, heavily carbon contaminated films were deposited at substrate temperatures between 450 and 550 °C. These films were identified via PXRD to be composed predominantly of $Bi_{24}Fe_2O_{39}$ and α-Fe_2O_3; postdeposition annealing at 550 °C resulted in visible removal of carbon contamination but also the evaporation of bismuth, to leave α-Fe_2O_3. Addition of air as an oxidizing gas during deposition resulted in films of predominantly $BiFeO_3$ only at a substrate temperature of 550 °C. Hematite (α-Fe_2O_3) was observed at 450 °C (see Supporting Information Figure S7) and was present at almost all growth temperatures. All films displayed good coverage, were red-orange in color, and could not be removed via tissue or scotch

DOI: 10.1021/acs.cgd.6b00370
Cryst. Growth Des. 2016, 16, 3818−3825

Table 1. Deposition Conditions for $BiFeO_3$ Thin Films Grown *via* LPCVD of $[Bi(O^tBu)_3]$ and $[Fe(acac)_3]$

Ref	Substrate Temp/°C	Bismuth source carrier gas flow rate/sccm	Iron source carrier gas flow rate/sccm	Air flow rate/sccm	Phase(s) obtained *via* XRD	Thickness/ nm	Band gap/eV	At. % Bi:Fe (from WDX)	At. % carbon (from WDX)
1	450	50	50	**0**	α-Fe_2O_3			9:81	6
2	475	50	50	**0**	$Bi_{24}FeO_{39}$ + α-Fe_2O_3			18:82	5
3	500	50	50	**0**	$Bi_{24}FeO_{39}$ + α-Fe_2O_3			28:72	16
4	550	50	50	**0**	$Bi_{24}FeO_{39}$ + α-Fe_2O_3			33:66	14
5	450	50	50	50	α-Fe_2O_3			5:95	<1
6	475	50	50	50	$Bi_{24}FeO_{39}$ + α-Fe_2O_3	370	2.0	29:71	4
7	500	50	50	50	$BiFeO_3$ + $Bi_{25}FeO_{40}$	520	2.2	34:66	3
8	550	50	50	50	$BiFeO_3$ + Fe_2O_3 + $Bi_{25}FeO_{40}$	650	2.2	47:53	2
9	575	50	50	50	$BiFeO_3$ + α-Fe_2O_3 + $Bi_{25}FeO_{40}$	860	2.1	44:56	<1
10	550	50	**40**	50	$BiFeO_3$ + $Bi_2Fe_4O_9$	920	2.3	54:46	<1
11	550	50	**25**	50	$BiFeO_3$ + $Bi_2Fe_4O_9$	580	2.1	57:43	1.6

tape. A summary of the deposition conditions and resultant films is displayed in Table 1.

Films deposited at 550 °C with both air bleed and N_2 carrier gas flow rates of 50 sccm (Lines 5−9, Table 1) possessed close to 1:1 ratios of Bi:Fe and were found to be predominantly composed of $BiFeO_3$ (Figure 3). Hexagonal unit cell parameters of a = 5.5680(4) Å, c = 13.841(1) Å (space group $R3c$) were obtained via unit cell refinement and were in agreement with literature values for bulk $BiFeO_3$ found via synchrotron X-ray diffraction (a = b = 5.57414(4) Å, c = 13.85882(12) Å, PDF = 014−0181).[19] Both $Bi_{25}FeO_{40}$ (isostructural to γ-Bi_2O_3 (PDF = 074−1375)) and α-Fe_2O_3 (PDF = 013−0534) were observed as impurity phases. It should be noted that the synthesis of phase-pure $BiFeO_3$ is very challenging and secondary phases (Fe_2O_3, $Bi_2Fe_4O_9$, $Bi_{25}Fe_4O_{39}$ etc.) are commonly observed in samples; other reports have attributed the intrinsic metastability of $BiFeO_3$, the ease of Bi_2O_3 evaporation, and the complex Bi_2O_3−Fe_2O_3 phase diagram as possible reasons for this phenomena.[20,21] In order to decrease the iron oxide content in the films, the carrier gas flow rate through the iron precursor, and hence molar transport, was decreased (Lines 10 and 11, Table 1). This resulted in the decrease in iron content in the films (Table 1) and disappearance of α-Fe_2O_3, but also led to emergence of a $Bi_2Fe_4O_9$ phase evident from XRD (see Supporting Information Figure S8). Film thicknesses were measured via side-on SEM imaging; the film growth rates are shown in the Supporting Information, Figure S9.

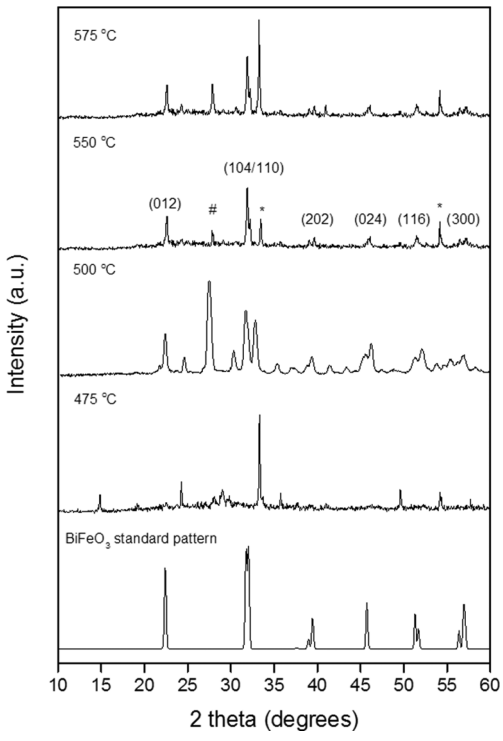

Figure 3. X-ray diffraction patterns of BFO films formed via LPCVD of $[Bi(O^tBu)_3]$, $[Fe(acac)_3]$, and air at various growth temperatures, using a 50 sccm gas flow rate for all sources; (*) correspond to α-Fe_2O_3, and (#) correspond to $Bi_{25}FeO_{40}$.

XPS measurements (Figure 4) in the iron 2p region revealed the expected $2p_{1/2}$ and $2p_{3/2}$ components at 723.8 eV and 711 eV, respectively; however, the latter peak was found to be broad and asymmetric and likely to be from α-Fe_2O_3, which made attempts at peak fitting problematic. A weak Fe^{3+} satellite peak was observed at ∼731 eV; furthermore, no evidence for Fe_3O_4 formation was shown.[22,23] XPS analysis of the surface bismuth 4f spectrum revealed two peaks corresponding to the Bi $4f_{7/2}$ region at 159.2 eV and the Bi $4f_{5/2}$ region at 164.5 eV (Figure 4b) which are both characteristic of Bi^{3+}.[24] For the oxygen 1s spectrum (Figure 4c) two peaks were noted at 530.1 eV, characteristic of metal oxide species, and at 532.4 eV, ascribed to surface OH.

SEM (Figure 5) was used to investigate the morphologies of films deposited using air as a coreactant. At 475 °C we observe distinct plate-shaped dense-packed crystallites of approximately 100 nm width. Upon increasing the deposition temperature, a slight increase in particle size to ∼150 nm was observed at 500 °C, and further increase of temperature resulted in coalescence of particles to create a very densely packed film, whereby it appears that the particle size decreases going up to 575 °C. The nucleation and growth rate are governed by independent parameters, although the rates are a function of both

DOI: 10.1021/acs.cgd.6b00370
Cryst. Growth Des. 2016, 16, 3818−3825

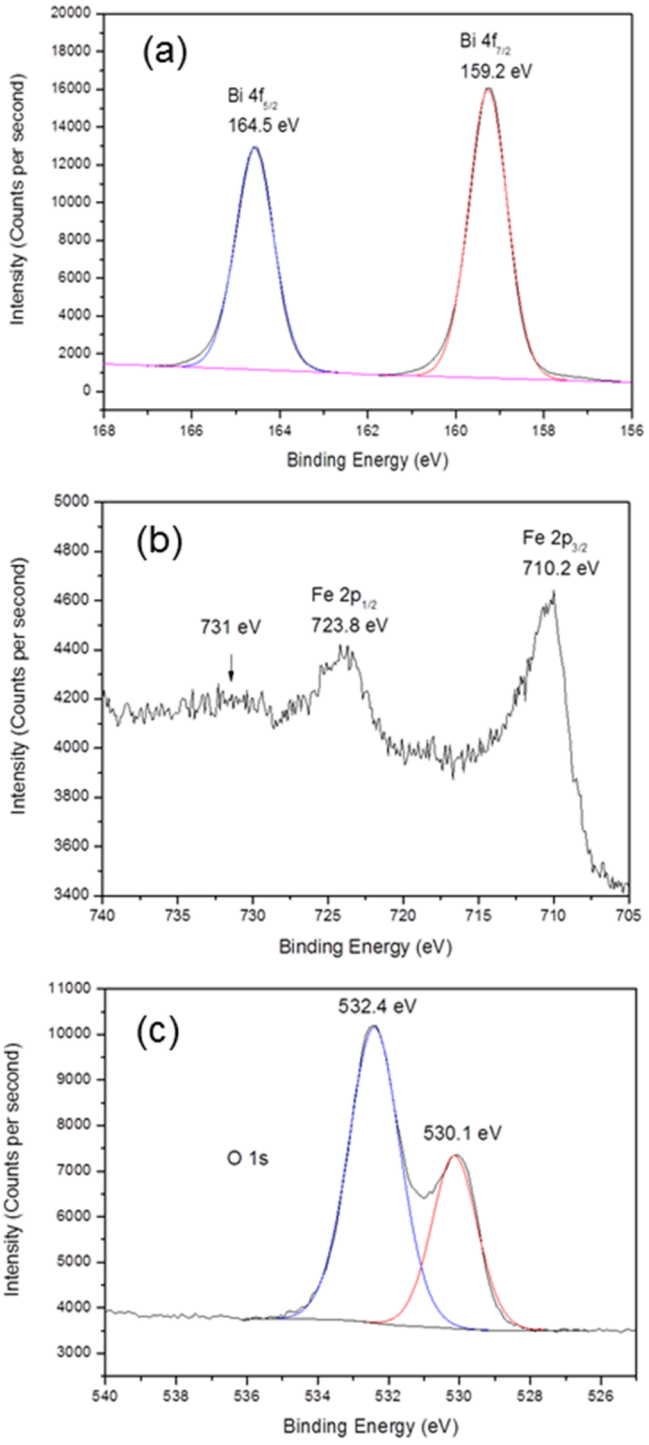

Figure 4. XPS spectra of (a) Bi 4f, (b) Fe 2p, and (c) O 1s regions in the $BiFeO_3$ film deposited at 550 °C via LPCVD.

temperature and precursor concentration; hence, this finding suggests the nucleation rate dominates as the growth temperature rises.[25] In all cases coverage was excellent. AFM analysis (see Supporting Information Figure S10) revealed that the root-mean-square (rms) roughness for a $BiFeO_3$ film deposited at 550 °C was ~30 nm, a little lower than that found for recently reported $BiFeO_3$ films synthesized by LPCVD (~60 nm).[26]

Raman spectra were collected for the $BiFeO_3$ samples deposited on glass substrates—peaks for $BiFeO_3$ were observed

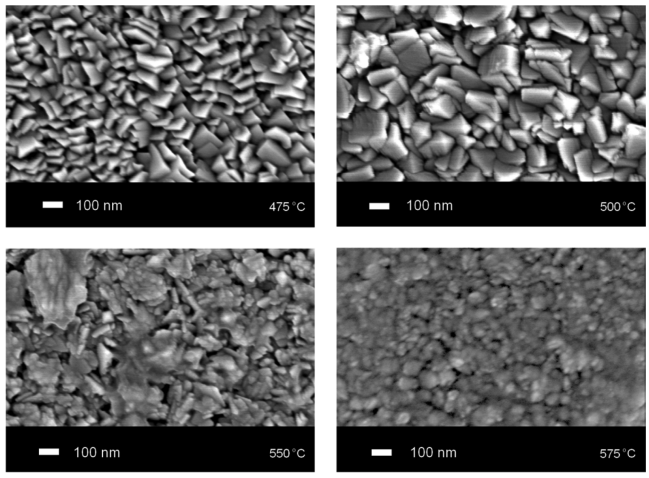

Figure 5. SEM images of $BiFeO_3$ films formed via LPCVD of $[Fe(acac)_3]$ and $[Bi(O^tBu)_3]$ and air at a variety of substrate temperatures.

at 147, 171, 221, 262, 277, 353, 482, 984, and 1106 cm^{-1} (see Figure 6).[27] The broad peak at 710 cm^{-1} remains unassigned.

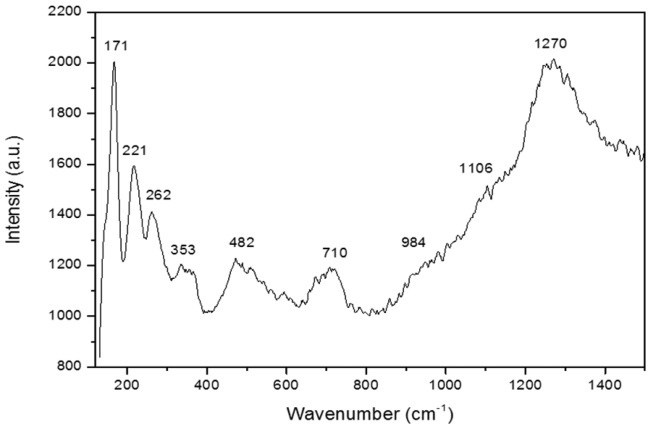

Figure 6. Room temperature Raman spectrum of the $BiFeO_3$ film deposited via LPCVD of $[Fe(acac)_3]$, $[Bi(O^tBu)_3]$, and air at 550 °C.

No peaks attributable to α-Fe_2O_3 were observed when we compared $BiFeO_3$ to α-Fe_2O_3 produced by LPCVD (see ESI Figure 11). From the literature, the A_1 modes are assigned to peaks at 147, 176, 227, and 490 cm^{-1}, while the E phonon modes of single crystal $BiFeO_3$ were observed at 77, 136, 265, 279, 351, 375, 437, 473, and 525 cm^{-1}, of which the peaks at 265, 279, and 353 cm^{-1} are consistent with peaks observed in our $BiFeO_3$ film.[28] The assignment of the relatively weaker peaks at 984 and 1106 cm^{-1} appears to originate from the two-phonon overtone modes ($2A_4$ and $2E_8$).[28]

Magnetic measurements were performed using a SQUID-VSM; the magnetic field was applied parallel to the sample, and M-H loops were measured at 5 K and at 300 K. The corrected magnetic moments were calculated by subtracting the diamagnetic/paramagnetic contribution to the M-H curve. The M-H hysteresis loop recorded at 5 K is shown in the Supporting Information (Figure S12) and exhibited weak ferromagnetic behavior with saturation magnetization of 130 emu/cm^3—much higher than that recorded by Thery (70 emu/cm^3) for 30 nm $BiFeO_3$ film grown on a $SrTiO_3$ substrate via CVD.[22] Given the small amount of α-Fe_2O_3 present, some

DOI: 10.1021/acs.cgd.6b00370
Cryst. Growth Des. 2016, 16, 3818−3825

net magnetization could be attributed to this phase. The coercivity was *ca.* 400 Oe at 5 K (see Figure S13, Supporting Information.) The M-H curve was also recorded at room temperature (Figure 7) and exhibited a large diamagnetic

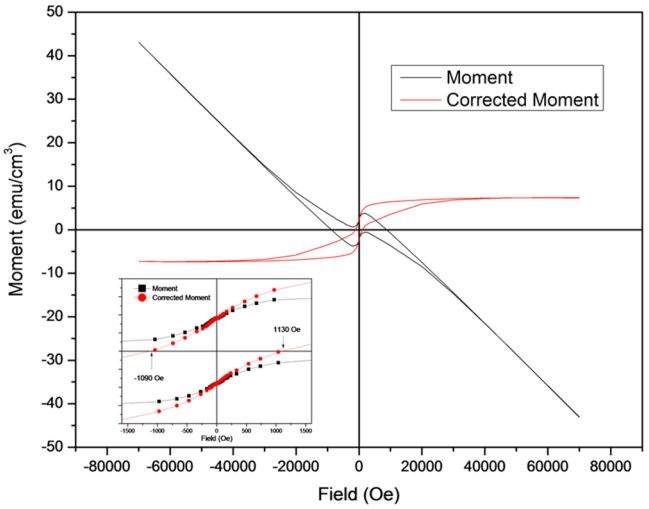

Figure 7. M-H hysteresis loop measured at 300 K for the predominantly $BiFeO_3$ film grown via LPCVD. The inset plot shows the M-H curve enlarged to display the coercive field of the sample.

contribution from the substrate, which was corrected. A saturation magnetization of 7.3 emu/cm^3 was recorded, which is similar to the calculated 7 emu/cm^3 value for bulk $BiFeO_3$.[29] The coercivity dramatically increased to ~1130 Oe, nearly three times that recorded for the same sample at the lower temperature. Estimation of the remnant ferroelectric polarization (P_r) proved challenging (see Supporting Information Figure S14), as the move to positive voltages caused a shift toward lower polarization values in the hysteresis loop; however, a P_r value of between 1 and 1.5 μC/cm^2 was measured. In summary, the observation of ferromagnetic and ferroelectric ordering at room temperature highlights that these $BiFeO_3$ films grown via CVD are multiferroic.

Photocatalysis. Band gaps for the as-deposited $BiFeO_3$ films were measured using Tauc plots from their UV−vis transmittance spectra (see Supporting Information Figures S15 and S16), and were found to be in the range 2.0−2.3 eV, as expected for $BiFeO_3$.[30] Previously we reported that $BiFeO_3$ showed excellent activity for photoelectrochemical water splitting under both visible and full spectrum irradiation, exhibiting Faradaic efficiency of over 80% under neutral conditions.[26] Here, we investigated whether the $BiFeO_3$ synthesized in this study could photo-oxidize water into gaseous oxygen under both full-arc and visible (λ > 420 nm) irradiation using silver ions as a sacrificial electron acceptor, and without electrical bias. As most of our LPCVD-grown films contained some α-Fe_2O_3 phase, as a control, a pure α-Fe_2O_3 (deposited at 450 °C) was tested for water oxidation under full arc irradiation, but no oxygen gas was detected by GC over 8 h of illumination due to the intrinsic high carrier recombination rate in hematite; thus, an electrical bias was required for efficient function.[31] Choosing a typical $BiFeO_3$ film deposited at 550 °C, oxygen gas from water photo-oxidation evolves steadily upon turning on the light source and continues for the duration of the experiment (Figure 8a). The initial O_2 evolution rate was almost linear at ca. 0.22 μmol/h. Silver metal is

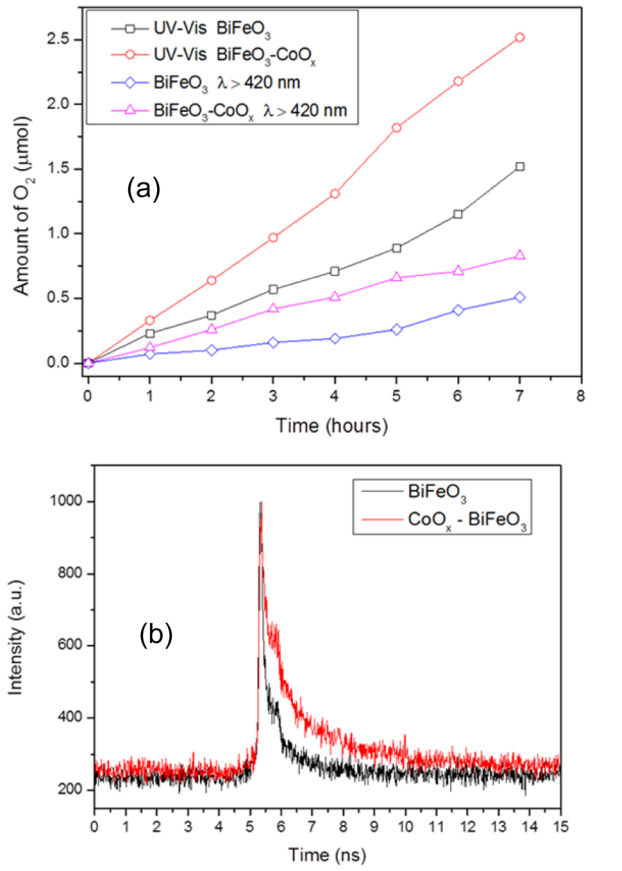

Figure 8. (a) Amount of O_2 evolved from $BiFeO_3$ and CoO_x-$BiFeO_3$ films under both full arc and visible irradiation using a $AgNO_3$ electron acceptor; (b) transient PL spectra of $BiFeO_3$ and CoO_x-$BiFeO_3$ measured at room temperature using an excitation wavelength of 432 nm.

deposited on the photocatalyst surface from the $AgNO_3$ electron acceptor ($Ag^+ + e^- \rightarrow Ag^0$) and can block incident photons and inhibit oxygen production; however, no decrease in gas evolution rate was observed over the 7 h time frame. This is likely due to the intrinsic low OER rate exhibited by $BiFeO_3$ for the kinetically slow four-hole water oxidation process; we expect that this would be an issue over a longer illumination period. Using a 420 nm long-pass filter, and thus under visible light illumination, oxygen evolution is also observed, albeit at a significantly lower rate (*ca.* 0.07 μmol/h) compared to full arc irradiation. This demonstrates that photocatalytic O_2 evolution on $BiFeO_3$ is predominantly a UV-driven process. In order to enhance charge separation and improve the surface kinetics for water oxidation,[4] a cobalt oxygen evolution catalyst was photodeposited on $BiFeO_3$ from $[Co(NO_3)_2]\cdot 6H_2O$ according to a published recipe.[32] XPS revealed the chemical state of cobalt to be predominantly +2 (see Supporting Information Figure S17). The resultant oxygen evolution under both full arc and visible irradiation exhibited a significant enhancement compared to the pure $BiFeO_3$, resulting in an initial OER of 0.38 μmol/h under full arc condition and 0.12 μmol/h under visible irradiation, altogether nearly double that of the unmodified $BiFeO_3$. The rates themselves are low compared to the most efficient water oxidation photocatalysts (e.g., $BiVO_4$, Ag_3PO_4)[33,34] because the total mass of CoO_x-$BiFeO_3$ present is not known and therefore an evolution rate per gram of photocatalyst cannot be stated with confidence; however, on

DOI: 10.1021/acs.cgd.6b00370
Cryst. Growth Des. 2016, 16, 3818−3825

a per meter basis the oxygen evolution rate would correspond to ~3800 μmol/m^2/h under full arc and ~1200 μmol/m^2/h under visible light irradiation. At 420 nm, a quantum efficiency of 2.1% was calculated for CoO_x-$BiFeO_3$, which is, to the best of our knowledge, the highest reported for a $BiFeO_3$ based oxygen evolving photocatalyst in the literature. Recently, a mesoporous $BiFeO_3$ was reported to have a high OER rate of 66 μmol/h/g,[35] while plasmonic enhanced Au/$BiFeO_3$ nanowires also showed appreciable oxygen evolution (ca. 20 μmol/h),[36] both under UV−vis irradiation and in the presence of sacrificial reagents. Thus, there is much promise for the use of polar photoferroic materials such as $BiFeO_3$ toward applications in solar energy conversion and renewable fuels synthesis.

To investigate the reasons for enhanced activity in our junction, time-resolved photoluminescence (PL) spectroscopy was used to measure the decay rate of radiative recombination in both materials (Figure 8b), using an excitation wavelength of 432 nm and pulse length of 50 μs.[37] The PL decay in the junction is almost two times slower than that of the unmodified $BiFeO_3$, indicating the more efficient charge separation brought about by the addition of CoO_x species.

CONCLUSIONS

We have synthesized a number of homoleptic bismuth(III) β-diketonate complexes as potential CVD precursors from which the crystal structure of [Bi(acac)$_3$] was elucidated to be comprised of a 1-D polymeric chain. TGA and evaporation experiments revealed poor volatilities and decomposition characteristics, and no BFO film growth was observed in conjunction with a volatile [Fe(acac)$_3$] iron source, using either LPCVD or AACVD. $BiFeO_3$ film growth via LPCVD was ultimately successful by replacing the bismuth diketonates with the volatile bismuth alkoxide [Bi(O^{t}Bu)$_3$], used together with [Fe(acac)$_3$] and air. Films were fully characterized via XRD, Raman, and WDX, which revealed close to a 1:1 stoichiometry for Bi:Fe at a growth temperature of 550 °C. Various levels of crystalline impurity phases were detected (e.g., α-Fe_2O_3, $Bi_{25}FeO_{40}$, and $Bi_2Fe_4O_9$) in some films. Magnetism experiments revealed weak ferromagnetic behavior while ferroelectric measurements revealed a low spontaneous polarization, but overall demonstrate that the films display multiferroic behavior at room temperature. $BiFeO_3$ has also been demonstrated to be an active water oxidation photocatalyst under both visible and full arc light irradiation in the presence of sacrificial reagents. Furthermore, it was found that the simple addition of a CoO_x cocatalyst enhances the charge separation and oxygen production. Nevertheless, it is clear that finding a ligand-matched volatile bismuth precursor for LPCVD film growth is still a challenge.

ASSOCIATED CONTENT

Supporting Information

The Supporting Information is available free of charge on the ACS Publications website at DOI: 10.1021/acs.cgd.6b00370.

Precursor synthesis and characterization details, crystal structure analysis, TGA analysis of precursors including PXRD of residues, vapor pressure curves, film growth rates, AFM, Raman spectra, M-H hysteresis curves (at 5 K), P-E plot, UV−vis spectra, Co 2p XPS spectra, and crystal data (PDF)

Accession Codes

CCDC 1458564 contains the supplementary crystallographic data for this paper. These data can be obtained free of charge via www.ccdc.cam.ac.uk/data_request/cif, or by emailing data_request@ccdc.cam.ac.uk, or by contacting The Cambridge Crystallographic Data Centre, 12 Union Road, Cambridge CB2 1EZ, UK; fax: +44 1223 336033.

AUTHOR INFORMATION

Corresponding Authors

*E-mail: s.moniz@ucl.ac.uk.
*E-mail: c.blackman@ucl.ac.uk.

Present Address

$^{\perp}$Department of Chemistry, Imperial College London, South Kensington Campus, London, SW7 2AZ, UK.

Notes

The authors declare no competing financial interest.

ACKNOWLEDGMENTS

UCL and EPSRC are thanked for a studentship. SM and JT acknowledge funding from EU-FP7 4G-PHOTOCAT (Project No. 309636). EPSRC are acknowledged for funding under research grants EP/F035675/1 and EP/N009533/1. We thank Dr. Graham Tizzard from the EPSRC National Crystallography Service for data collection.

REFERENCES

(1) Schultz, A. M.; Zhang, Y.; Salvador, P. A.; Rohrer, G. S. *ACS Appl. Mater. Interfaces* **2011**, *3*, 1562−1567.
(2) Li, L.; Salvador, P. A.; Rohrer, G. S. *Nanoscale* **2014**, *6*, 24−42.
(3) Butler, K.; Frost, J. M.; Walsh, A. *Energy Environ. Sci.* **2015**, *8*, 838−848.
(4) Moniz, S.; Shevlin, S. A.; Martin, D.; Guo, Z.; Tang, J. *Energy Environ. Sci.* **2015**, *8*, 731−759.
(5) Moniz, S. J. A.; Quesada-Cabrera, R.; Blackman, C. S.; Tang, J.; Southern, P.; Weaver, P. M.; Carmalt, C. J. *J. Mater. Chem. A* **2014**, *2*, 2922−2927.
(6) Marchand, P.; Hassan, I. A.; Parkin, I. P.; Carmalt, C. J. *Dalton Transactions* **2013**, *42*, 9406−9422.
(7) Tiitta, M.; Niinistou, L. *Chem. Vap. Deposition* **1997**, *3*, 167−182.
(8) Kang, S.; Rhee, S. W. *Thin Solid Films* **2004**, *468*, 79−83.
(9) Moniz, S. J. A.; Bhachu, D.; Blackman, C. S.; Cross, A. J.; Elouali, S.; Pugh, D.; Quesada Cabrera, R.; Vallejos, S. *Inorg. Chim. Acta* **2012**, *380*, 328−335.
(10) Hatanpää, T.; Vehkamäki, M.; Ritala, M.; Leskelä, M. *Dalton Transactions* **2010**, *39*, 3219−3226.
(11) Maeda, K.; Teramura, K.; Lu, D.; Takata, T.; Saito, N.; Inoue, Y.; Domen, K. *Nature* **2006**, *440*, 295.
(12) Serpone, N. *J. Photochem. Photobiol., A* **1997**, *104*, 1−12.
(13) Massiani, M.-C.; Papiernik, R.; Hubert-Pfalzgraf, L. G.; Daran, J.-C. *Polyhedron* **1991**, *10*, 437−445.
(14) Armelao, L.; Bandoli, G.; Casarin, M.; Depaoli, G.; Tondello, E.; Vittadini, A. *Inorg. Chim. Acta* **1998**, *275-276*, 340−348.
(15) Dikarev, E. V.; Zhang, H.; Li, B. *J. Am. Chem. Soc.* **2005**, *127*, 6156−6157.
(16) Stavila, V.; Dikarev, E. V. *J. Organomet. Chem.* **2009**, *694*, 2956−2964.
(17) Brooks, K. C.; Turnipseed, S. B.; Barkley, R. M.; Sievers, R. E.; Tulchinsky, J. V.; Kaloyerosj, A. E. *Chem. Mater.* **1992**, *4*, 912−916.
(18) Pisarevsky, A. P.; Martynenko, L. I. *Russian Journal of Coordination Chemistry* **1994**, *20*, 303−327 (English translation)..
(19) Reyes, A.; Delavega, C.; Fuentes, M.; Fuentes, L. *J. Eur. Ceram. Soc.* **2007**, *27*, 3709−3711.
(20) Valant, M.; Axelsson, A.; Alford, N. *Chem. Mater.* **2007**, *19*, 5431−5436.

DOI: 10.1021/acs.cgd.6b00370
Cryst. Growth Des. 2016, 16, 3818−3825

(21) Ramirez, F. E. N.; Pasca, G. A. C.; Souza, J. A. *Phys. Lett. A* **2015**, *379*, 1549−1553.
(22) Thery, J.; Dubourdieu, C.; Baron, T.; Ternon, C.; Roussel, H.; Pierre, F. *Chem. Vap. Deposition* **2007**, *13*, 232−238.
(23) Mocherla, P. S. V.; Karthik, C.; Ubic, R.; Ramachandra Rao, M. S.; Sudakar, C. *Appl. Phys. Lett.* **2013**, *103*, 022910.
(24) Sarala Devi, G. *Sens. Actuators, B* **1999**, *56*, 98−105.
(25) Ling, M.; Blackman, C. *Physica Status Solidi (C)* **2015**, *12*, 869−877.
(26) Moniz, S. J. A.; Blackman, C. S.; Southern, P.; Weaver, P. M.; Tang, J.; Carmalt, C. J. *Nanoscale* **2015**, *7*, 16343−16353.
(27) Rout, D.; Moon, K.-S.; Kang, S.-J. L. *J. Raman Spectrosc.* **2009**, *40*, 618−626.
(28) Ramirez, M. O.; Krishnamurthi, M.; Denev, S.; Kumar, A.; Yang, S.-Y.; Chu, Y.-H.; Saiz, E.; Seidel, J.; Pyatakov, A. P.; Bush, A.; Viehland, D.; Orenstein, J.; Ramesh, R.; Gopalan, V. *Appl. Phys. Lett.* **2008**, *92*, 022511.
(29) Ederer, C.; Spaldin, N. *Phys. Rev. B: Condens. Matter Mater. Phys.* **2005**, *71*, 1−4.
(30) Luo, J.; Maggard, P. A. *Adv. Mater.* **2006**, *18*, 514−517.
(31) Townsend, T. K.; Sabio, E. M.; Browning, N. D.; Osterloh, F. E. *Energy Environ. Sci.* **2011**, *4*, 4270.
(32) Li, R.; Han, H.; Zhang, F.; Wang, D.; Li, C. *Energy Environ. Sci.* **2014**, *7*, 1369−1376.
(33) Kudo, A.; Ueda, K.; Kato, H.; Mikami, I. *Catal. Lett.* **1998**, *53*, 229−230.
(34) Martin, D.; Liu, G.; Moniz, S.; Bi, Y.; Beale, A.; Ye, J.; Tang, J. *Chem. Soc. Rev.* **2015**, *44*, 7808−7828.
(35) Papadas, I.; Christodoulides, J. A.; Kioseoglou, G.; Armatas, G. S. *J. Mater. Chem. A* **2015**, *3*, 1587−1593.
(36) Li, S.; Zhang, J.; Kibria, M. G.; Mi, Z.; Chaker, M.; Ma, D.; Nechache, R.; Rosei, F. *Chem. Commun.* **2013**, *49*, 5856−5858.
(37) Sheu, Y. M.; Trugman, S. A.; Park, Y.-S.; Lee, S.; Yi, H. T.; Cheong, S.-W.; Jia, Q. X.; Taylor, A. J.; Prasankumar, R. P. *Appl. Phys. Lett.* **2012**, *100*, 242904.

DOI: 10.1021/acs.cgd.6b00370
Cryst. Growth Des. 2016, 16, 3818−3825